Songklanakarin J. Sci. Technol.
44 (2), 534-541, Mar. - Apr. 2022

http://www.sjst.psu.ac.th

Original Article

Conceptualizing the parallax of movement control orders (MCOs) to the spatial dispersion of PM_{10}

Noraain Mohamed Saraf[1], Nursyahreen Aqilah Mohmad Rassid[2], Siti Aekbal Salleh[1, 3*], Nurul Amirah Isa[1], Ameerah Su'ad Abdul Shakor[4, 5], and Muhammad Alfatih Pahrol[4]

[1] *Centre of Studies for Surveying Science and Geomatics, Faculty of Architecture, Planning and Surveying, Universiti Teknologi MARA, Shah Alam, Selangor, 40450 Malaysia*

[2] *Examap Sdn Bhd, Ukay Perdana, Ampang, Selangor, 68000 Malaysia*

[3] *Institute for Biodiversity and Sustainable Development, Universiti Teknologi MARA, Shah Alam, Selangor, 40450 Malaysia*

[4] *Environmental Health Research Center, Institute for Medical Research, National Institutes of Health Malaysia, Ministry of Health Malaysia, Shah Alam, Selangor, 40170 Malaysia*

[5] *Public Health Division, Selangor State Health Department, Ministry of Health Malaysia, Shah Alam, Selangor, 40100 Malaysia*

Received: 28 July 2021; Revised: 11 October 2021; Accepted: 5 November 2021

Abstract

Due to the COVID-19 pandemic, many countries have implemented movement control orders (MCO). Globally, including in Malaysia, such bans have reduced pollution. Thus, this study used remote sensing to examine the particle dispersion and intensity of PM_{10}. Unlike previous research, this technique used Landsat 8 Operational Land Imager (OLI) satellite images to estimate anthropogenic level changes within the study area. Eight models are used to estimate PM_{10} levels. The models work well because they were developed and tested in India, which has a similar climate to Malaysia. Two models returned results that matched the study area's CAQMs station. Between 10th March 2020 and 26th March 2020 the CAQMS showed an average PM_{10} concentration of 17-32 g/m^3. The pixel based PM_{10} estimation is 30-35% off in g/m^3. However, the percent reduction of PM_{10} before and during MCO was within 2% of Model 5 and 7. Incorporating geospatial technology into baseline studies to assess current air quality is clearly beneficial. Since the first MCO in March 2020, toxic pollution emissions have decreased significantly.

Keywords: PM_{10} concentration, MCO, Malaysia, remote sensing, GIS

1. Introduction

Malaysia first experienced haze in April 1983, disrupting daily life. It is estimated that eight million hectares of land burned annually produce 30% of global average annual greenhouse gas emissions. The worst haze in Malaysian history occurred in Kuching, where the API exceeded 850 (Hanafi, Hassim & Noor, 2018). The occurrence of haze has had a detrimental effect on the well-being of the people living in and around countries such as Singapore and Brunei. Apart from the direct effects on human health, such as breathing difficulties and vomiting, Malaysian schools have been ordered to close. According to 2010 data, the number of daily hospital visits increased by 31% during the Kuala Lumpur haze episode. Johor is another state in Malaysia that was severely impacted by the haze episode caused by the Indonesian forest fires. According to Hamid, Rahmat & Sapani (2018), during the Southwest Monsoons of 2011 and 2013, the air quality in Larkin and Pasir Gudang was classified as unsafe and harmful when particulate matter

*Corresponding author
Email address: aekbal@uitm.edu.my

concentrations in the air reached 54.12 g/m^2 during the dry season and 56.83 g/m^2 during the wet season. However, during normal periods, open burning, vehicle exhaust emissions, and industrial wastes account for the majority of Malaysia's air pollution (Sentian, Jemain, Gabda, Franky & Wui, 2018).

Meanwhile, the first case of coronavirus disease 2019 (COVID-19) was discovered near Wuhan, China, and the sickness quickly spread throughout the country. Following that, news of COVID-19, which was first discovered on tourists from Hubei, China, on 25th January 2020, horrified Malaysia (Elengoe, 2020). Due to the dramatic surge in instances, Malaysia's Prime Minister issued a Movement Control Order (MCO), which puts a halt to all transportation and movement into and out of the country. This also limited and slowed local business travel, as well as closing institutions, colleges, and schools to prevent illness spread and establishing quarantines (Nadzir *et al*., 2020). The Movement Control Order (MCO) enforcement not only helped to break the COVID-19 chain, but it also helped to reduce pollution by reducing common activities including open burning, traffic density, industrial stack emissions, and nitrogen dioxide (NO_2) pollution (Abdullah *et al*., 2020). In Malaysia, measuring the results of major concentrations of air pollutants including particulate matter (PM_{10}), is defined as the Air Pollutant Index (API).

Nevertheless, in Malaysia, a daily mean of ozone (O_3), carbon monoxide (CO), nitrogen dioxide (NO_2), and particulate matter (PM_{10}) has been found to be strongly related with natural mortality (Hanafi *et al*., 2018). These pollutants can induce heart disease, chronic lung illness, and acute lung disease, as well as exacerbate existing lung conditions like asthma and bronchitis (Manisalidis Stavropoulou, Stavropoulos & Bezirtzoglou, 2020). As a result, efforts to monitor air quality are required to keep the public informed about the current state of air quality and public health concerns. However, due to the differences in air pollutant measurements, this study will solely focus on the PM_{10} indicator because PM will be a significant parameter for the air quality index (AQI) value during the haze period.

The changes in air pollutants caused by COVID-19 are nearly unreachable, making it difficult to create a map and effectively communicate the facts of COVID-19 effects to the public. It has been feasible to track how decreases in released particle emissions affect the concentration of air pollution using modern technology such as geographic information system (GIS), which shows layers of complex data on maps. It may also be able to determine the levels of air pollution in a certain place, as well as how they compare to surrounding areas. In this scenario, image satellite-based remote sensing can aid in research and development. These technologies allow multiple physical features to be observed continuously across large areas, with an observational density proportionate to the sensor's spatial resolution. As a result, remote sensing can be utilized to estimate PM_{10} concentrations and provide geographically continuous data (Fernandez-Pacheco *et al*., 2018).

Many researches have utilized satellite images to predict the concentration of PM_{10}, with strong coefficients of determination between estimated and ground-level PM_{10} concentrations (Gayen, Haque & Mishra, 2021; Hung, Ahn, Linh, Binh & Hoang, 2018; Pambudi *et al*., 2020; Saraswat, Mishra & Kumar, 2017). Therefore, the primary source of information for estimating air pollutants measurement can be exposures to develop a GIS model to estimate PM_{10} reading directly from remotely sensed data (Somvanshi, Vashisht, Chandra & Kaushik, 2019). In general, an air pollution map with adequate distribution can be displayed using air quality stations. A study and assessment to measure air pollutants concentration by air monitoring stations and display the distribution using satellite images are lacking in Pasir Gudang despite the ambient air quality being established. Thus, the COVID-19 pandemic has not only brought a new normal in the lives of the society, but it has also breathed new life into the environment (Rupani *et al*., 2020).

According to Abdullah *et al*. (2020), the MCO has a significant effect on reducing particulate matter concentrations in Malaysia. The study suggests that future research should include factors like weather, traffic density, industrial activity, and biomass burning. Insufficient ground station coverage in Malaysia may also affect estimates of particulate matter values for the entire study area. Furthermore, development within 10km of ground stations may affect PM_{10} readings (Latif *et al*., 2014). The lack of monitoring stations makes mapping PM_{10} concentrations in these highly affected areas difficult. Thus, this study employs a new modelling approach using satellite images and mathematical models to improve the coverage of PM_{10} data sources.

2. Study Area

The study area is at Johor Bahru (128° 13’ N, 103° 54’ 10” E) in southern Peninsular Malaysia. Johor Bahru has 497,097 residents and a 220 km^2 study area. It is a major center for manufacturing, logistics, and commerce. This location was chosen for its pollution issues. Johor Bahru is one of the largest cities in Malaysia. The population of Johor Bahru is very high given the job opportunities in Singapore; making this city to expand rapidly. People daily commutes to Singapore was the focus of the study to see the effects of PM_{10}. Furthermore, this study area has large business districts that occupied by factories which were not allowed to be operated during MCO. Due to this condition, this area is suitable to study the effects of MCO on the PM_{10} distribution.

3. Data Acquisition

OLI images from Landsat 8 were used. Landsat 8 OLI data is used to image process the distribution of air quality. The satellite images were obtained from the USGS's Earth Explorer website (http://earthexplorer.usgs.gov). For this study, we chose only two images, dated 10th March 2020 (collection 1) and 26th March 2020 (collection 2). These dates were selected due to clear sky view. The image captured on 26th March 2020 was selected during the early MCO period. During this date, Malaysia is having total lockdown phase, thus, offering a very conducive environment that suits this study’s objectives. This study was conducted in the early implementation of MCO in Malaysia which makes the effects of PM_{10} to be significant since very little personal transports were given the permission to be on-road.

4. Methodology

Erdas Imagine and ArcGIS were used to prepare the PM_{10} data layers using Landsat 8 OLI satellite images. Using Erdas Imagine, PM_{10} values were extracted from satellite images and ArcGIS for analysis and mapping. This study has four main stages. Figure 1 depicts the study's four major stages.

4.1 Radiometric correction and calibration

Every sensor in the outer space needs to be calibrated according to their characteristics to ensure that the digital number of every pixel represent the actual condition of the Earth surface. This calibration is needed due to the interactions of the wavelength with the substances contained in the atmosphere. As suggested by the data provider, the selected satellite images should be calibration prior to analyses (Isa, Wan Mohd, Salleh & Ooi, 2018).

4.1.1 TOA algorithm (Conversion of DN to TOA radiance)

OLI data can be converted to TOA spectral radiance using the radiance rescaling factors provided in the metadata file. Equation 1 was used to convert DN values to TOA radiance.

$$L_\lambda = M_L * Q_{cal} + A_L \quad (1)$$

where L_λ is the TOA spectral radiance (Watts/ (m^2 * srad * μm)), M_L is the band-specific multiplicative rescaling factor from the metadata (RADIANCE_MULT_BAND_x, where x is the band number), A_L is the band-specific additive rescaling factor from the metadata (RADIANCE_ ADD_BAND_x, where x is the band number), and Q_{cal} is the quantized and calibrated standard product pixel values (DN).

4.1.2 Conversion of TOA radiance to TOA reflectance

Then, the top of atmosphere reflectance (TOA) was calculated from top of radiance layer. It can be calculated using reflectance rescaling coefficients provided in the product metadata file (MTL file). Equation 2 was used to convert DN values to TOA reflectance:

$$p_\lambda = M_p * Q_{cal} + A_p \quad (2)$$

where P_λ is the TOA planetary reflectance, without correction for solar angle (Note that ρλ' does not contain a correction for the sun angle), Mρ is the band-specific multiplicative rescaling factor from the metadata (Reflectance_ Mult_Band_x, where x is the band number), Aρ is the band-specific additive rescaling factor from the metadata (Reflectance_Add_Band_x, where x is the band number), and Qcal is the quantized and calibrated standard product pixel values (DN).

Due to the sun radiation effects on the satellite images, the calculated surface reflectance layer must be adjusted using sun angle correction equation to eliminate the errors contained.

$$\rho\lambda = \frac{\rho\lambda'}{cos(\theta_{SZ})} = \frac{\rho\lambda'}{sin(\theta_{SE})} \quad (3)$$

where ρλ is the TOA planetary reflectance, θ_{SE} is the local sun elevation angle (The scene center sun elevation angle in degrees is provided in the metadata (SUN_ELEVATION)), and Θ_{SZ} is the local solar zenith angle; $\theta_{SZ} = 90° - \theta_{SE}$.

4.1.3 Scaling factor of landsat 8 collection

Landsat sensors offer various type of end products. These products come with scaling factor to enhance its quality for various analyses purposes. Hence, the scaling factor should be considered prior to further data processes. As for this study, Landsat 8 OLI Collection 1 and Collection 2 were used for 10th March 2020 and 26th March 2020 respectively. The scaling factor for both images are as follows:

Table 1. Scale factor

Surface reflectance	Scale factor collection 1	Scale factor collection 2
	0.0001	0.0000275 +-0.2 (Additional offset of -0.2 per pixel)

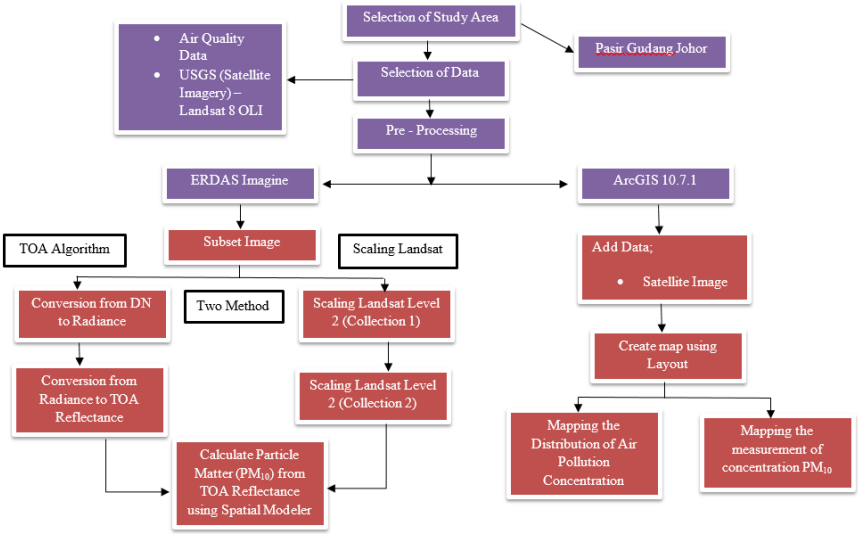

Figure 1. Flowchart of the methodology

4.2 Estimation of PM_{10} values

PM_{10} values of the study area was extracted from Landsat 8 OLI satellite images. Developed PM_{10} models by Saraswat *et al*. (2017) were used to predict PM_{10} concentrations over Johor at Pasir Gudang Johor. PM_{10} maps were generated, dated between 10th March 2020 and 26th March 2020 during MCO. The models were employed due to similar climate experiences in both studies. Thus, these models are suitable to be tested in this study. The models were also verified to have high accuracy on their performance in tropics. Even though some of them were tested to have lower accuracy, a few of them can be used to estimate PM_{10} with reliable results.

4.2.1 Aerosol Optical Thickness (AOT) and PM_{10}

The reflectance measured from the satellite images (reflectance at the top of the atmospheric, TOA) were subtracted by the amount of the surface reflectance to prepare atmospheric reflectance. The algorithm of AOT for single band or wavelength (λ) is simplified as:

$$AOT(\lambda) = a_o R(\lambda) \quad (4)$$

The interaction between PM_{10} and AOT is derived from a single homogeneous atmospheric layer comprising spherical aerosol particles. It can then be expected that the PM parameter would be more explicitly associated with AOT. Using the information collected by the spectral AOT extraction, a system has been developed to retrieve particulate matter concentrations. By substituting AOT in term of PM_{10}, into the equation (5), the algorithm of PM_{10} with spectral reflectance of multi-band wavelengths (λ) is simplified as:

$$AOT(\lambda) = a_j R_{\lambda 1} + a_j R_{\lambda 2} + a_j R_{\lambda 3} + a_j R_{\lambda 4} \ldots . (5)$$

where $R_{\lambda 1}$ is the atmospheric reflectance (i = 1, 2 and 3 corresponding to wavelength for satellite), and a_j is the algorithm coefficient (j = 0, 1 and 2).

4.2.2 PM_{10} concentration using models developed by Saraswat *et al*. (2017)

In Saraswat *et al*. (2017), eight models were developed based on the aerosol optical reflectance model which are capable to estimate PM_{10} values. By utilizing the properties of visible bands, the models were proved to offer reliable estimation of PM_{10} values. The study examined the linear relationship (using regression model) between particulate matter concentration and the atmospheric reflectance within visible band range. The study further showed that satellite imagery can provide continuous monitoring over a large coverage area. Table 2 shows the eight models adopted to explore the implications of the enforced MCO to the PM_{10} values over the study area.

5. Results and Analysis

In this section, the PM_{10} distribution within the study area and how MCO affected the concentration were analyzed. This study exhibited that despite of many negative impacts of COVID-19 and the enforcement of MCO to the socio-economic activities and health, our nation also gaining some benefits. By looking at the effects and impacts of this event at different perspectives, one may gain new insight and the situation can be totally the opposite. One may perceive as negatives, while other perspectives one may gaining benefit. Hence this is parallax. The following sections, separate the results based on two objectives i.e. the estimation of pixel based PM_{10} concentrations as well as looking at the models performances by comparing the values of the PM_{10} with the continuous air quality monitoring station (CAQMs) situated nearby the study area. Then, investigation of the dispersion patterns before and during MCO can be visualized.

5.1 Estimating pixel-based particulate matter concentrations

The adopted mathematical models depicted a well spatial coverage in particulate matter (PM) of the study area. Two dates; 10th March 2020 and 26th March 2020 were utilized, and the results can be seen in Table 3 and Figure 2. The values of minimum and maximum of the calculated PM are significantly different according to the models. Thus, point out the necessity of the local climate parameter calibration and specific physic options for the study area, including the calibration towards the spectral bands (Table 3). Cloud cover is one of the detected issues that influenced such variance in the calculated values.

A large variance can be seen across the models. Based on the daily observation made by the continuous air quality monitoring station (CAQMs) the daily minimum and maximum of the nearest station is 13.75 and 58.85 for 10th March 2020 and 5.91 and 24.65 for 26th March 2020 respectively. Although, the models show good accuracy in the initial study performed by Saraswat *et al*. (2017), Table 3 suggested the models 1, 2, 6 and 8 have underestimated, while models 3, 4, 5 and 7 overestimated the values of PM_{10}.

Table 2. Models to estimate PM_{10} from landsat 8 (Saraswat *et al*., 2017)

Model	Mathematical Model	R	RMSE (μg/m^3)
1.	PM10 = RBand1(24.45) – 83.4119	0.8627	24.5811
2.	PM10 = RBand2(28.12) – 34.9272	0.8829	22.8210
3.	PM10 = RBand3(35.81) + 60.0301	0.8648	24.4000
4.	PM10 = RBand4(40.92) + 108.845	0.8325	26.9231
5.	PM10 = RBand1(− 25.78) + RBand2(59.89) + 24.1226	0.8899	22.1712
6.	PM10 = RBand2(43.45) + RBand3(− 20.12) – 84.0814	0.88552	22.5824
7.	PM10 = RBand3(64.39) + RBand4(− 34.41) + 25.5796	0.8728	23.7157
8.	PM10 = RBand1(− 53.69) + RBand2(134.26) + RBand3(− 60.70) – 60.248	0.9050	20.6694

The over/under calculated condition may be due to several factors; geographical setting of the study area, reflective properties of the earth surface, atmospheric and climatic condition of the study area, the physics condition of the study area (vapors and cloud properties) as well as the over correction parameters of spectral band.

The spatial distribution of PM_{10} over the study area can be seen in Figure 2. Based on these maps, it is exhibited that land use land cover (LULC) also influenced the dispersion and intensity of PM_{10} (Yuan, 2008; Chen *et al*., 2021). Apart from the known meteorological parameters that evidently plays an important role in the dispersion of PM_{10}. These models can be further calibrated by fusing the localized condition of the climatic parameters, meteorological parameters, topographic conditions and also the anthropogenic condition of the study area.

5.2 Pattern of PM_{10} phase before and during movement control order

The estimated pixel based PM_{10} prior to the date before enforcement of MCO (10th March) and during the MCO (26th March), daily PM_{10} concentrations were in the range of 47.9–136.77 μg/m^3 and 25.82–110.50 μg/m^3 respectively. The New Malaysia Ambient Air Quality Standard (NMAAQS) has set the standard PM_{10} limit to 100 μg/m^3 for an average of 24 hours (Department of Environment Malaysia **[**DOE**]**, 2020) and the World Health Organization (WHO) (2018) has set a stricter PM_{10} limit to 50 μg/m^3. Among the models explored four of them return with illogical results which the writer would assume that it is due to the external and physical factors of how the models were established originally at different region and locational setting. Of course this initial assumption will need further investigations. However, another four models show a promising similarity in term of trends (Table 4). Larger differences in term of its average values, probably caused by the over corrected satellite image**'**s electromagnetic radiation values. Table 4 shows PM_{10} concentration differences before and during MCO of the four models.

Based on the reading from Table 4, Model 5 shows the highest reduction percentage of 47.14% from 48.85 μg/m^3 before the MCO to 25.82 μg/m^3 during the MCO. Followed by Model 7 with reduction of 43.36% to bring the PM_{10} values before MCO at 47.94 to 27.15 μg/m^3. This estimation is about 30%-35% overestimated from the observed values based on the *μg/m^3*. Despite this, two (2) models (Model 5 and 7) show a remarkable agreement in term of their percentage (%) reduction, which are 47.17% and 43.36% respectively as compared with the observed values percentage reduction at 45.15%. Thus, with this reasonable evidence, one could conclude that pixel based PM_{10} estimation can give a reasonable indication or instrument for baseline impacts study in relation to the air quality monitoring at a moderate scale. Furthermore, the results also suggested that the enforcement of MCO/EMCO has successfully reduced the emissions of pollutants, especially the PM_{10} concentration, which was directly due to the decreased of motor vehicles on the roads and economic industrial activities during this period (Abdullah *et al*., 2020).

The following maps shows the spatial distribution of PM_{10} is mostly concentrated in the east, and west and especially in the central region of Johor, following major roads and urban nuclei, where PM_{10} even exceeds the annual average limit for human health protection set as 50 μg/m^3. The distribution for PM_{10} indicates that the most affected areas are areas in the southern and eastern provinces but without exceeding the set annual average limit. These maps also show the transition PM_{10} intensity moving towards the rural zones away from large agglomerations signify the activities are more localized perhaps within the allowable radius distance according to the government SOP. According to Abdullah *et*

Table 3. Estimated particle matter

Dates	10 March 2020 (observed)		26 March 2020 (observed)	
No. Algorith	Min (13.75)	Max (58.85)	Min (5.91)	Max (24.65)
Model 1	-89.41	-34.19	-88.30	-62.85
Model 2	-34.92	21.15	-40.55	-10.14
Model 3	60.03	131.58	52.86	91.66
Model 4	108.84	195.14	100.66	146.86
Model 5	24.12	92.57	17.30	55.21
Model 6	-84.08	-36.15	-88.74	-63.57
Model 7	25.57	83.51	19.58	50.52
Model 8	-60.24	-17.14	-64.22	-39.35

Table 4. Average PM_{10} values before-during MCO

Model no.	Average of emission of PM_{10} before and during MCO			
	10 March 2020 before MCO (31.95 μg/m3) 61	26 March 2020 during MCO (17.43 μg/m3) 46.5	Variation	
			μg/m^3 (-17.52)	Change (%) (-54.84%)
Model 3	85.53	61.68	-23.85	-27.88
Model 4	136.77	110.50	-26.27	-19.20
Model 5	48.85	25.82	-23.03	-47.14
Model 7	47.94	27.15	-20.79	-43.36

al. (2020), there has been a 26% increase in the good Air Pollution Index (API) days throughout Malaysia since the MCO began. MCO not only reduces the spread of COVID-19 among community members but also reduces environmental pollution due to reduced anthropogenic activity.

With uniform scale range, Figures 3-6 illustrates the spatial distribution of PM_{10} estimated by models 3, 4, 5, and 7. Strong agreement in term of the dispersion and distribution of the values of PM_{10} can be visually examined throughout the maps.

6. Conclusions

The algorithms used were adopted from Saraswat *et al.* (2017). Among these models, two had given a good estimation of the PM_{10} concentrations at the study area. The study proved the efficiency of utilizing the multispectral bands of satellite images to estimation the PM_{10} concentration. With remote sensing and GIS not only that the estimation can be made with reasonable accuracy but also with good spatial coverage and resolution. It enables us to leverage on the

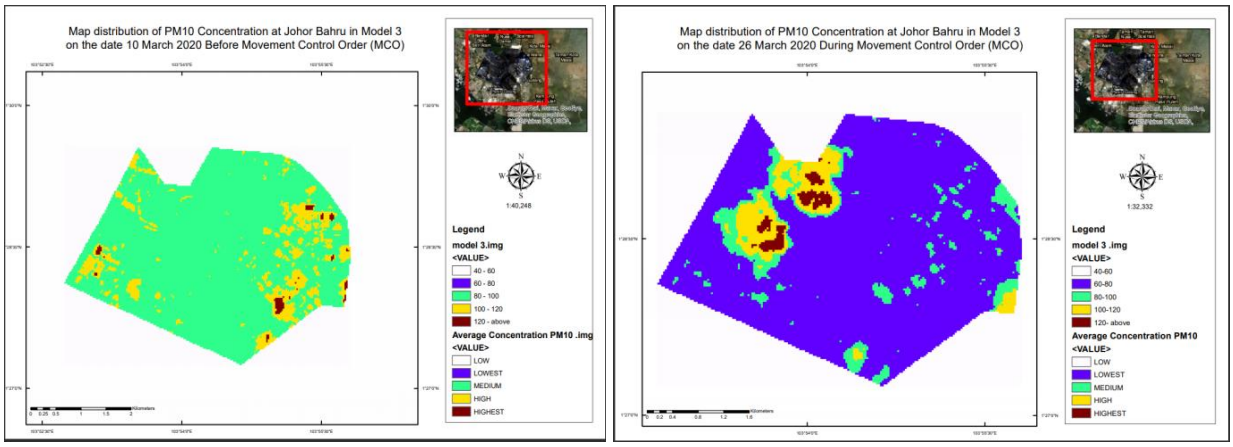

Figure 3. PM_{10} distribution map before and during MCO in model 3

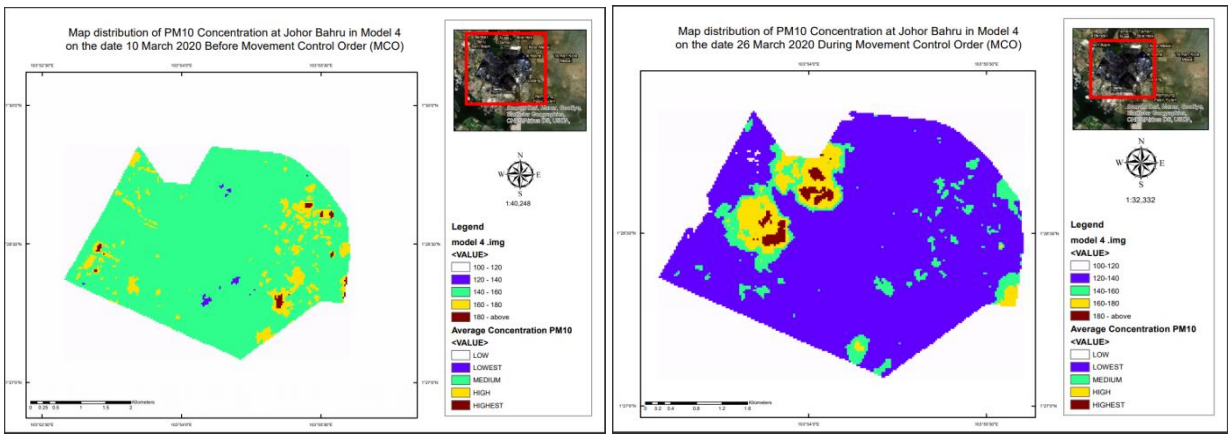

Figure 4. PM_{10} distribution map before and during MCO in model 4

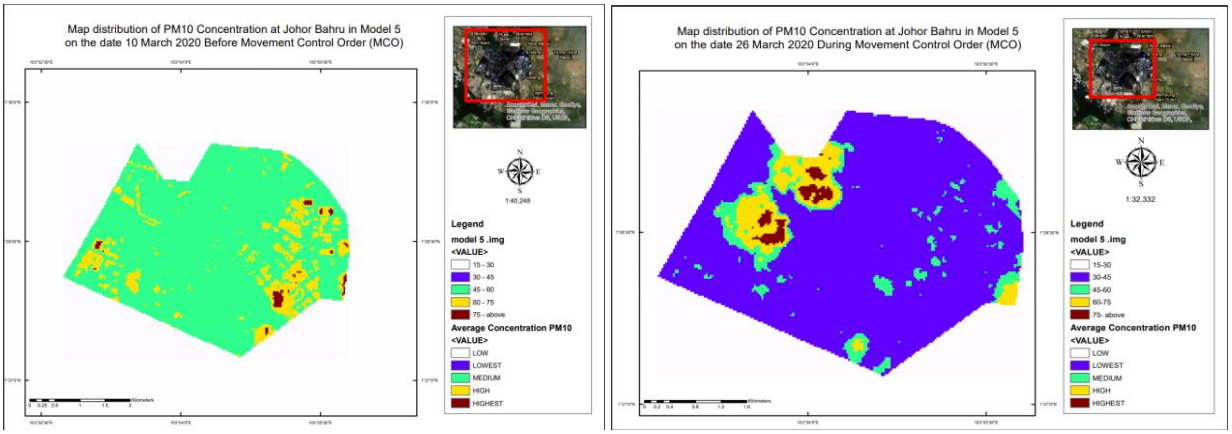

Figure 5. PM_{10} distribution map before and during MCO in model 5

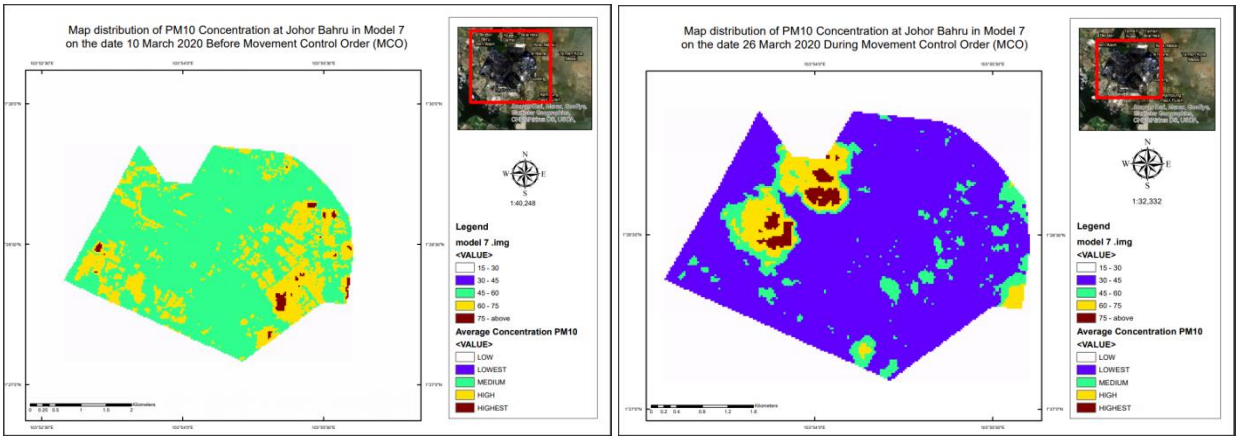

Figure 6. PM_{10} distribution map before and during MCO in model 7

existing data archive that are easily accessed and downloadable without any cost. Not only that this is cost effective, but it is also helping in making an informed decision. It can be concluded that based on the eight models, two of them are giving a reasonably good result to represent the condition of study area with the percentage (%) reduction variance of ±2%. With some calibrations and further investigation, in fine tuning the 30-35% overestimated $\mu g/m^3$ values of PM_{10}, perhaps it can potentially be the best to represent the study area. In the future, perhaps more in-situ observations and data can be prepared to support the development of a robust model that will give flexible to the for environmental researcher to utilize by providing a dynamic and scalable calibration and physics option.

Acknowledgements

The author would like to gratefully acknowledge financial support from Universiti Teknologi MARA and the Ministry of Health Malaysia under the Research Grant of Ministry of Health Malaysia, NMRR-19-3747-52136.

References

Abdullah, S., Mansor, A. A., Napi, N. N. L. M., Mansor, W. N. W., Ahmed, A. N., Ismail, M., & Ramly, Z. T. A. (2020). Air quality status during 2020 Malaysia Movement Control Order (MCO) due to 2019 novel coronavirus (2019-nCoV) pandemic. *Science of the Total Environment*, *729*, 139022

Chen, C. Y., Chen, H. W., Sun C. T., Chuang, Y. H., Nguyen, K. L. P. & Lin, Y. T. (2021). Impact assessment of river dust on regional air quality through integrated remote sensing and air quality modelling. *Science of The Total Environment*, *755*(2), 142621

Department of Environment. (2020). *Enforcement the compliance of EQ* (*Scheduled waste*) *Regulation 2005 through system eSWIS*,**"** pp. 1–2, 2020

Elengoe A. (2020). COVID-19 Outbreak in Malaysia. *Osong Public Health and Research Perspectives 2020*, *11*(3), 93-100

Fernandez-Pacheco, V. M., López-Sánchez, C. A., Álvarez-Álvarez, E., López, M. J., García-Expósito, L., Yudego, E. A., & Carús-Candás, J. L. (2018). Estimation of PM_{10} distribution using Landsat5 and Landsat8 remote sensing. *In Proceeding of the Multidisciplinary Digital Publishing Institute* (Volume 2, No. 23, p. 1430). doi:10.3390/proceedings2231430

Gayen, A., Haque, S. M., & Mishra, S. V. (2021). COVID-19 induced lockdown and decreasing particulate matter (PM_{10}): An empirical investigation of an Asian megacity. *Urban Climate*, *36*, 100786. doi:10.1016/j.uclim.2021.100786

Hamid, H. A., Rahmat, M. H., & Sapani, S. A. (2018). The classification of PM_{10} concentrations in Johor Based on Seasonal Monsoons. *In IOP Conference Series*: *Earth and Environmental Science* (Volume 140, No. 1, p. 012028).

Hanafi, N. H., Hassim, M. H., & Noor, Z. Z. (2018). Overview of health impacts due to haze pollution in Johor, Malaysia. *Journal of Engineering and Technological Sciences*, *50*(6)., 818-831. doi:10.5614/j.eng.technol.sci.2018.50.6.5

Hung, N. N., Anh, V., Linh, P. H., Binh, N. T. & Hoang, V. V. (2018). Determining PM_{10} model in Hanoi using Landsat 8 oil and ground-measured dust data. *VNU Journal of Science*: *Earth and Environmental Sciences*, *34*. doi:10.25073/2588-1094/vnuees.4146.

Isa, N. A., Wan Mohd, W. M. N., Salleh S. A. & Ooi, M. C. G. (2018). The effects of green areas on air surface temperature of the Kuala Lumpur city using WRF-ARW modelling and remote sensing technique. *IOP Conference Series*: *Earth and Environmental Science*, *117*, 012012

Latif, M. T., Dominick, D., Ahamad, F., Khan, M. F., Juneng, L., Hamzah, F. M. & Nadzir, M. S. M. (2014). Long term assessment of air quality from a background station on the Malaysian peninsula. *Science of the Total Environment*, *482*, 336–348. doi:10.1016/j.scitotenv.2014.02.132

Manisalidis, I., Stavropoulou, E., Stavropoulos, A., & Bezirtzoglou, E. (2020). Environmental and health impacts of air pollution: A review. *Frontiers in Public Health*, *8*. doi:10.3389/fpubh.2020.00014

Nadzir, M. S. M., Ooi, M. C. G., Alhasa, K. M., Bakar, M. A. A., Mohtar, A. A. A., Nor, M. F. F. M., . . . Nor, M. Z. M. (2020). The impact of movement control

order (MCO) during pandemic COVID-19 on local air quality in an urban area of Klang valley, Malaysia. *Aerosol and Air Quality Research*, *20*(6), 1237-1248

Pambudi, R. A., Naldi, A., Luthfi, A., Puspitarini, D.A., Chaerani, M.M., Permana, M.W. & Shafira, S. (2020). Spatiotemporal trend of particulate matter (PM_{10}) concentration on cement industries in Klapanunggal and Citeureup Sub-districts. *In IOP Conference Series*: *Earth and Environmental Science* 561, doi:10.1088/1755-1315/561/1/012035

Rupani, P. F., Nilashi, M., Abumalloh, R. A., Asadi, S., Samad, S., & Wang, S. (2020). Coronavirus pandemic (COVID-19) and its natural environmental impacts. *International Journal of Environmental Science and Technology*, 1-12. doi:10.1007/s13762-020-02910-x

Saraswat, I., Mishra, R. K., & Kumar, A. (2017). Estimation of PM_{10} concentration from Landsat 8 OLI satellite imagery over Delhi, India. *Remote Sensing Applications*: *Society and Environment*, *8*, 251-257

Sentian, J., Jemain, M. A., Gabda, D., Franky, H., & Wui, J. C. H. (2018). Long-term trends and potential associated sources of particulate matter (PM_{10}) pollution in Malaysia. *WIT Transactions on Ecology and the Environment*, 230, 607-618. doi:10.2495/AIR180571

Somvanshi, S. S., Vashisht, A., Chandra, U., & Kaushik, G. (2019). *Delhi air pollution modeling using remote sensing technique*. *Handbook of Environmental Materials Management*. Basel, Switzerland: Springer Nature. doi:10.1007/978-3-319-58538-3_174-1

Yuan, F. (2008). Land-cover change and environmental impact analysis in the Greater Mankato area of Minnesota using remote sensing and GIS modelling. *International Journal of Remote Sensing*, *29*(4)